The Crystal Structure of NAD(P)H Quinone Oxidoreductase 1 in Complex with Its Potent Inhibitor Dicoumarol†

Gad Asher,‡ Orly Dym,§ Peter Tsvetkov,‡ Julia Adler,‡ and Yosef Shaul*,‡

Departments of Molecular Genetics and Structural Biology, Weizmann Institute of Science, Rehovot 76100, Israel

Received January 3, 2006; Revised Manuscript Received March 1, 2006

ABSTRACT: NAD(P)H quinone oxidoreductase 1 (NQO1) is a ubiquitous flavoenzyme that catalyzes two-electron reduction of quinones to hydroquinones utilizing NAD(P)H as an electron donor. NQO1 binds and stabilizes several short-lived proteins including the tumor suppressors p53 and p73 and the enzyme ornithine decarboxylase (ODC). Dicoumarol is a widely used potent competitive inhibitor of NQO1 enzymatic activity, which competes with NAD(P)H for binding to NQO1. Dicoumarol also disrupts the binding of NQO1 to p53, p73, and ODC and induces their ubiquitin-independent proteasomal degradation. We report here the crystal structure of human NQO1 in complex with dicoumarol at 2.75 Å resolution. We have identified the interactions of dicoumarol with the different residues of NQO1 and the conformational changes imposed upon dicoumarol binding. The most prominent conformational changes that occur in the presence of dicoumarol involve Tyr 128 and Phe 232 that are present on the surface of the NQO1 catalytic pocket. On the basis of the comparison of the NQO1 structure in complex with different NQO1 inhibitors and our previous analysis of NQO1 mutants, we propose that the specific conformation of Tyr 128 and Phe 232 is important for NQO1 interaction with p53 and other client proteins.

NAD(P)H quinone oxidoreductase 1 (NQO1)[1] is a ubiquitous flavoenzyme that catalyzes two-electron reduction of various quinones utilizing NAD(P)H as an electron donor (*1*). NQO1-mediated reduction of quinones to hydroquinones is an important cellular defense mechanism against oxidative stress (*2*). In addition to its role in the detoxification of quinones, the enzyme catalyzes the reductive activation of quinolic chemotherapeutic compounds such as mitomycins and β-lapachone (*3*, *4*). Studies of NQO1 structure and function have shown that NQO1 is a homodimer that functions via a "ping-pong" mechanism. NAD(P)H binds to NQO1, reduces the FAD cofactor, and is then released, allowing the quinone substrate to bind the enzyme and to be reduced. The NAD(P)H and the quinone binding sites of NQO1 have a significant overlap, thus providing a molecular basis for this ping-pong mechanism (*5*).

Certain coumarins, flavones, and the reactive dye Cibacron blue are competitive inhibitors of NQO1 activity, which compete with NAD(P)H for binding to NQO1. Dicoumarol [3,3′-methylenebis(4-hydroxycoumarin)] is the most potent competitive inhibitor of NQO1 with a K_i of 1−10 nM (*6*). Dicoumarol competes with NAD(P)H for binding to NQO1 and prevents the electron transfer to FAD (*6*). Other coumarins [warfarin and esculetin (6,7-dihydroxycoumarin)] (*7*), flavones [phenindione, chrysin, and DHF (7,8-dihydroxyflavone)] (*8*, *9*), and Cibacron blue (*9*, *10*) are less potent inhibitors of NQO1 than dicoumarol and appear to bind differently to the enzyme. The K_i for NQO1 inhibition by Cibacron blue is 170 nM. Another NQO1 inhibitor, ES936 (5-methoxy-1,2-dimethyl-3-[(4-nitrophenoxy)methyl]indole-4,7-dione), is a mechanism-based inhibitor with a K_i of 450 nM. The inhibition of NQO1 by ES936 is NADH-dependent and involves the generation of reactive iminium species that alkylate a tyrosine residue of NQO1 (*11*). Recently, we have found that curcumin, a natural phenolic compound found in the spice turmeric, also inhibits NQO1 activity (*12*).

In addition to its role in the detoxification of quinones, NQO1 is also a 20S proteasome-associated protein that plays an important role in the stability of the tumor suppressor p53 and several other short-lived proteins including p73α and ornithine decarboxylase (ODC) (*13*−*20*). NQO1 binds and stabilizes p53, protecting p53 from ubiquitin-independent 20S proteasomal degradation (*16*, *18*, *21*). Dicoumarol and several other inhibitors of NQO1 activity, which compete with NADH for binding to NQO1, disrupt the binding of NQO1 to p53 and induce ubiquitin-independent p53 degradation (*16*, *18*). However, the molecular basis of NQO1 association and dissociation from p53 and its other client proteins is unknown. Studying the structure of NQO1 in a complex with dicoumarol, a complex that is impaired in protein binding (p53, p73α, and ODC) might provide important insight into the mechanism of NQO1 interaction with p53 and its other client proteins.

Several studies investigated the binding of dicoumarol to NQO1 using site-directed mutagenesis, inhibitor binding analysis, and computer modeling, but a definitive structure of NQO1 bound to dicoumarol has not yet been resolved

† This work was supported by grants from the Israel Academy of Sciences and Humanities and the Samuel Waxman Cancer Research Foundation.

* Corresponding author. Phone: 972-8-9342320. Fax: 972-8-9344108. E-mail: yosef.shaul@weizmann.ac.il.

‡ Department of Molecular Genetics, Weizmann Institute of Science.

§ Department of Structural Biology, Weizmann Institute of Science.

[1] Abbreviations: NQO1, NAD(P)H quinone oxidoreductase 1; NADH, nicotinamide adenine dinucleotide phosphate; ODC, ornithine decarboxylase; FAD, flavin adenine dinucleotide; DHF, 7,8-dihydroxyflavone; PMSF, phenylmethanesulfonyl fluoride; PEG, poly(ethylene glycol); Ni-NTA, nickel nitrilotriacetic acid; TEV, tobacco etch virus; DMSO, dimethyl sulfoxide.

10.1021/bi0600087 CCC: $33.50
Published on Web 04/26/2006

Table 1: Summary of the Crystallographic Data Collection and Analysis

Crystal Parameters	
space group	P_1
unit cell	
a (Å)	76.24
b (Å)	86.19
c (Å)	100.56
α (deg)	91.14
β (deg)	107.91
γ (deg)	93.17
Data Collection	
resolution range (Å)	40−2.75
no. of observations	325967
no of unique reflections	63333
completeness (%)[a]	96.9 (95.2)
$\langle I\rangle/\langle\sigma(I)\rangle$	7.6 (2)
R on *I* (%)	9.4 (35.3)
refinement and model statistics	
total no. of reflections	61222
no. of reflections in test set	6220
water molecules	400
R (%)[b]	22.5
R_{free} (%)[c]	26.9
Stereochemical Parameters	
RMSD from ideal values	
bond lengths (Å)	0.009
bond angles (deg)	1.4
torsion angles (deg)	21.5
improper torsion angles (deg)	0.98
estimated coordinate error	
low-resolution cutoff (Å)	5
ESD from Luzzati plot (Å)[d]	0.37
ESD from SIGMAA (Å)	0.48
Ramachandran plot	
residues in most favored regions (%)	84.2
residues in additionally allowed regions (%)	15.0
residues in disallowed regions (%)	0.4

[a] Last resolution shell 2.8−2.75 Å. [b] $R = \sum||F_o| - |F_c||/\sum|F_o|$, where F_o denotes the observed structure factor amplitude and F_c the structure factor calculated from the model. [c] R_{free} is for 10% of the randomly chosen reflections excluded from the refinement. [d] ESD, estimated standard deviation.

(*9*, *22*). In this study, we report the crystal structure of human NQO1 complexed with dicoumarol at 2.75 Å resolution. By analyzing the crystal structure, we have identified the interactions of dicoumarol with the different residues of NQO1 and the consequent conformational changes. In addition, comparison of the NQO1 structures in complex with different NQO1 inhibitors led us to propose a model whereby the conformation of two key NQO1 residues present on the surface of the NQO1 catalytic pocket, Tyr 128 and Phe 232, may determine the binding affinity of NQO1 to p53 and to other client proteins.

MATERIALS AND METHODS

Purification of Recombinant NQO1. BL21(DE3) bacteria expressing pET28-His-TEV-NQO1 were lysed by sonication in 50 mM Tris-HCl, pH 7.5, 150 mM NaCl, and 1 mM PMSF. Soluble His-TEV-NQO1 was purified using a Ni-NTA column (HiTrap chelating HP) followed by gel filtration chromatography (HiLoad 16/60 Superdex 200). Purified His-TEV-NQO1 was then cleaved by TEV protease, and the His-TEV was removed upon binding to a Ni-NTA column.

Crystallization and Data Collection. Single crystals of NQO1 with dicoumarol were obtained by the microbatch method under oil, using the IMPAX 1-5 robot (Douglas Instruments, East Garston, Hungerford, Berkshire, U.K.). The protein was crystallized at a concentration of 10 mg/mL. Crystals of NQO1−dicoumarol were grown from a precipitating solution of 0.2 M NaOAc, 190 mM Na-Tricine, pH 8.1, and 22% PEG 3350 with 10 mM dicoumarol in 1% DMSO. A complete data set was collected from a single crystal on a Rigaku R-AXIS IV++ imaging plate area detector using a Rigaku RU-H3R rotating anode operated at 5 kW and osmic multilayer X-ray focusing mirrors. Diffraction data were integrated, scaled, and reduced using the HKL program package (*23*). Crystals formed in space group P_1, with cell constants $a = 76.24$ Å, $b = 86.19$ Å, $c = 100.56$ Å, $\alpha = 91.14°$, $\beta = 107.91°$, and $\gamma = 93.17°$. The crystals contain four dimers in the asymmetric unit cell with a V_m of 2.6 Å^3/Da and diffracted to 2.75 Å resolution. The structure was solved by molecular replacement using the program PHASER (*24*) by using the refined structure of a native NQO1 dimer (1DXO in the Protein Data Bank) as a model. Atomic refinement was carried out with the program CNS (*25*). Map display and model rebuilding were performed using the program O (*26*) and model inspection using WHATIF and PROCHECK (*27*). The figures were created using the program PyMOL. The atomic coordinates of the NQO1−dicoumarol crystal structure were deposited in the Protein Data Bank (PDB accession code 2F1O).

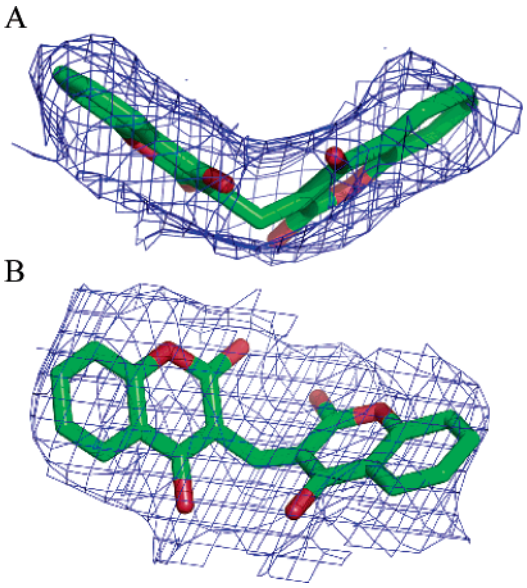

FIGURE 1: Electron density map of dicoumarol. (A) Omit electron density map ($F_o - F_c$) in the dicoumarol binding site contoured at 3σ level at 2.75 Å resolution. (B) Omit electron density map of dicoumarol approximately 90° rotated around the *X*-axis. Carbon atoms are colored in green; oxygen atoms are colored in red.

RESULTS

Structure Determination and Refinement. The crystal structure of the hNQO1 in complex with dicoumarol was determined at 2.75 Å resolution and was refined to *R*-values of 22.5% and R_{free} values of 26.9% with good stereochemistry (Table 1). Final maps show good density for most portions of the polypeptide chains including the FAD and the bound dicoumarol (Figure 1).

Crystal Structure of the hNQO1−Dicoumarol Complex. NQO1 is a physiological homodimer composed of two

FIGURE 2: Overall structure of the hNQO1 homodimer with dicoumarol. Ribbon representation of the human NQO1 homodimer with FAD and dicoumarol. FAD colored in red and dicoumarol colored in blue are shown in stick representation.

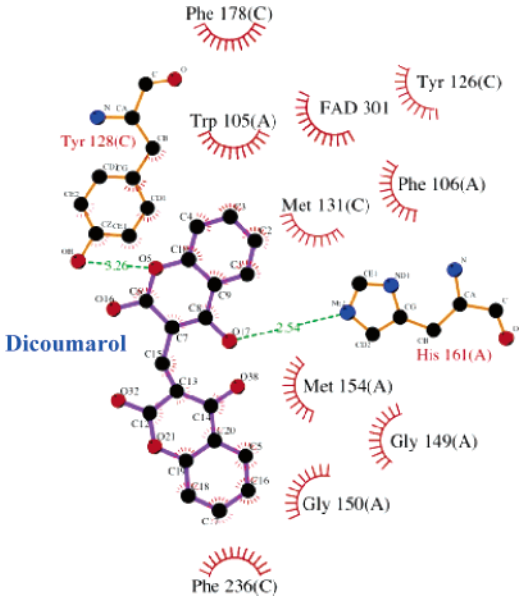

FIGURE 3: Schematic representation of dicoumarol/hNQO1 interactions. Protein amino acid residues and FAD and dicoumarol molecules are labeled (C and A refer to the first and second NQO1 monomers, respectively). Nitrogen atoms are colored in blue, oxygen atoms are colored in red, and carbon atoms are colored in black. Hydrogen bonds are represented by dashed green lines along with their distances. Residues making hydrogen bonds together with dicoumarol are shown in stick representation. Residues making van der Waals interactions with the inhibitor are represented by a decorated arc. The schematic representation was created using the program LigPlot (*29*).

interlocked monomers of 273 residues related by a noncrystallographic 2-fold axis of symmetry. Each monomer is composed of two domains: a large catalytic domain with α/β fold with flavodoxin topology (residues 1−220) and a small C-terminal domain (residues 221−273). Two catalytic sites are formed and are present at the dimer interface. Two FAD molecules are present; each one is bound to the catalytic domain of each monomer. The FAD moiety in the catalytic domain of one of the monomers forms one wall of the catalytic pocket, while residues from both monomers generate the other walls (*5*, *28*).

Dicoumarol is a competitive inhibitor of NQO1 with respect to NAD(P)H (*6*). Our hNQO1−dicoumarol structure shows that dicoumarol is bound to each of the catalytic sites interacting with FAD and with residues from both monomers (Figure 2). The plane of dicoumarol stacks parallel to the isoalloxazine ring of the FAD that forms one of the walls of the catalytic pocket. The average distance between the planes of the two rings is 4 Å. Dicoumarol binds to the active site through a series of hydrophobic and hydrogen bonds with residues from both monomers and the FAD (Figure 3). One coumarin ring of dicoumarol makes two hydrogen bonds: O5 of dicoumarol with the OH of Tyr 128 of the first monomer and the O17 of dicoumarol with the Nϵ of His 161 of the second monomer (Figure 3).

Comparison of the Structure of the hNQO1−Dicoumarol Complex with Apo hNQO1. Alignment of the apo hNQO1 dimer (PDB accession code 1D4A) with hNQO1 in complex with dicoumarol yields 0.36 RMS deviation for the 546 α-carbon atoms. The structural changes associated with dicoumarol binding occur on several residues involving both monomers. Maximal movement is observed with Tyr 128 and Phe 232 of the first monomer (Figure 4A). The distance between these two residues increases from about 5 Å in the apo hNQO1 to about 12 Å in the hNQO1−dicoumarol complex (Table 2). Other residues exhibit more limited movement and include Phe 236 of the first monomer and Phe 106 and His 161 of the second monomer. The FAD molecule and Tyr 126 (not shown) adopt identical conformations in both apo hNQO1 and hNQO1−dicoumarol structures (Figure 4A). The allosteric changes in residues Tyr 128 and Phe 232 of hNQO1 upon binding of dicoumarol are clearly apparent on the surface of NQO1 (Figure 5; compare panels A and C).

Comparison of the Structure of the hNQO1−Dicoumarol Complex with the hNQO1−Duroquinone Complex. NQO1 catalyzes two-electron reduction of quinones to hydroquinones. The crystal structure of hNQO1 with duroquinone (2,3,5,6-tetramethyl-*p*-benzoquinone), an NQO1 substrate, was previously determined (PDB accession code 1DXO). Duroquinone binds to the active site through a series of interactions involving the FAD and several hydrophobic and hydrophilic residues (*28*). The duroquinone stacks parallel 3.5 Å from the isoalloxazine ring of the FAD, forming hydrogen bonds with Tyr 126, Tyr 128, and His 161 (*28*). Alignment of hNQO1 dimer in complex with duroquinone with the hNQO1 in complex with dicoumarol yields 0.33 RMS deviation for the 546 α-carbon atoms. The major differences observed between the two structures involve the positions of Tyr 128 and Phe 232 of the first monomer (Figure 4B). The distance between these two residues increases significantly from about 4 Å in the hNQO1 in complex with duroquinone to about 12 Å in the NQO1−dicoumarol complex (Table 2). The position of Tyr 128 and Phe 232 in the apo hNQO1 and the hNQO1 in complex with duroquinone is similar (Figure 5; compare panels A and B).

Comparison of the Structure of the hNQO1−Dicoumarol Complex with the hNQO1−ES936 Complex. The quinone ES936 is a mechanism-based inhibitor of NQO1. ES936 undergoes NADH-dependent reduction by NQO1 followed by the loss of *p*-nitrophenol, generating a reactive iminium species that alkylates either Tyr 126 or Tyr 128, resulting in irreversible inactivation of the enzyme. The structure of

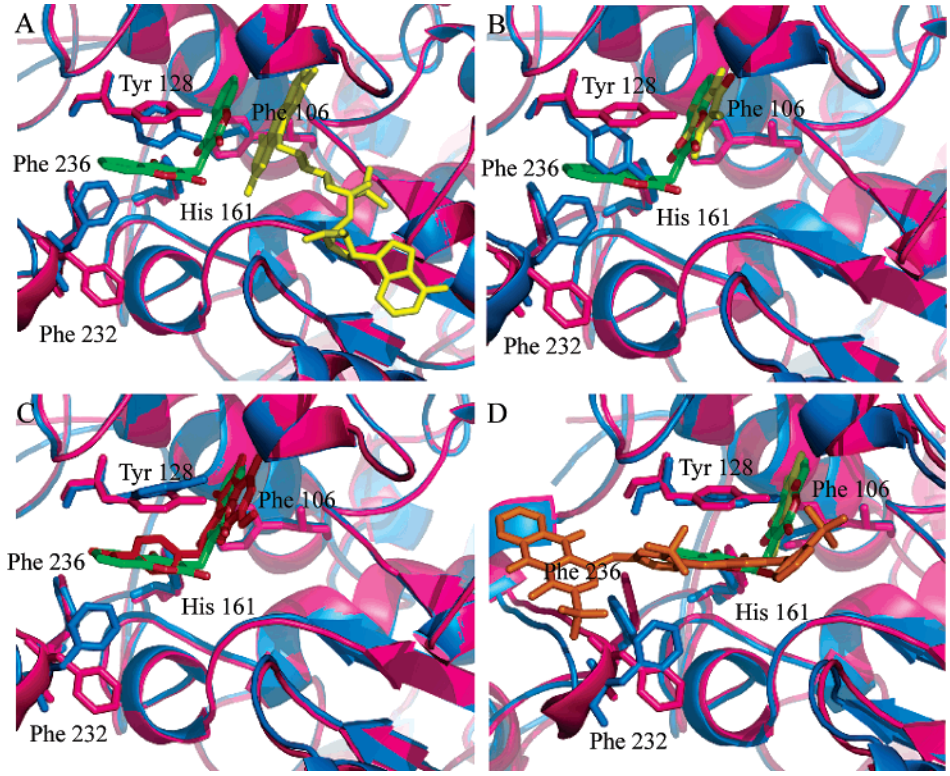

FIGURE 4: Comparison of the binding of different inhibitors and a substrate to the active site of NOQ1. (A) Superposition of the active site of hNQO1 in complex with dicoumarol colored in pink with the apo hNQO1 (PDB accession code 1D4A) colored in blue. Dicoumarol is colored in green; FAD is colored in yellow. (B) Superposition of the active site of hNQO1 in complex with dicoumarol colored in pink with the hNQO1 in complex with duroquinone (PDB accession code 1DXO) colored in blue. Dicoumarol is colored in green; duroquinone is colored in yellow. (C) Superposition of the active site of hNQO1 in complex with dicoumarol colored in pink with the hNQO1 in complex with ES936 (PDB accession code 1KBQ) colored in blue. Dicoumarol is colored in green;ES936 is colored in red. (D) Superposition of the active site of hNQO1 in complex with dicoumarol colored in pink with the rat NQO1 in complex with Cibacron blue (PDB accession code 1QRD) colored in blue. Dicoumarol is colored in green; Cibacron blue is colored in orange. Residues of the active site, FAD, the different inhibitors, and a substrate are represented in stick representation.

Table 2: Summary of the Major Distances and Hydrogen Bonds within the NQO1 Active Site upon Binding of the Different Inhibitors and a Substrate

	distance (Å)		
substrate/inhibitor	Tyr 128−Phe 232	FAD−isoallozaxine ring	hydrogen bonds
dicoumarol	12	4	Tyr 128, His 161
duroquinone (*28*)	4	3.5	Tyr 126, Tyr 128, His 161
ES936 (*11*)	8	3.6	Tyr 126
Cibacron blue (*5*)	9	5.4	Tyr 128, Phe 232

hNQO1 in complex with ES936 was previously resolved (PDB accession code 1KBQ). The ES936 stacks parallel to the isoalloxazine ring of the FAD and interacts with FAD and residues from both monomers (*11*). The enzyme−inhibitor interactions are mostly hydrophobic contacts, with only one hydrogen bond between the indolequinone O7 and Tyr 126 (*11*). Alignment of the hNQO1 dimer in complex with ES936 with the hNQO1−dicoumarol complex yields 0.45 RMS deviation for the 546 α-carbon atoms. The only apparent change in the presence of ES936 is in the position of Phe 232 (Figure 4C). The movement of Phe 232 upon binding of ES936 is more limited compared to the effect of dicoumarol. The distance between Tyr 128 and Phe 232 is about 8 Å in the hNQO1−ES936 complex, while the distance in the hNQO1−dicoumarol complex increases to about 12 Å (Table 2). The relative positions of Phe 232 and Tyr 128 are again highlighted on the surface of NQO1 (Figure 5; compare panels C and D).

Comparison of the Structure of the hNQO1−Dicoumarol Complex with the Rat NQO1−Cibacron Blue Complex. Cibacron blue is a water-soluble triazine dye that binds to the nucleotide-binding site of many enzymes. It is a competitive inhibitor of NQO1 with respect to NAD(P)H with a K_i of 170 nM. The crystal structure of the rat NQO1 together with duroquinone and Cibacron blue (PDB accession code 1QRD) shows that Cibacron blue interacts with residues from both NQO1 monomers (*5*). Alignment of the rat NQO1 dimer in complex with Cibacron blue and duroquinone with the human NQO1−dicoumarol complex yields 0.75 RMS deviation for the 546 α-carbon atoms. The distance between residues Tyr 128 and Phe 232 increases from about 4 Å in the hNQO1−duroquinone complex to about 9 Å in the rat NQO1 in complex with Cibacron blue together with duroquinone (Table 2). The movement of Tyr 128 and Phe 232 in the case of Cibacron blue is reduced compared to the changes that occur in the presence of dicoumarol (Table 2). However, in contrast to dicoumarol and ES936, the three ring moieties of Cibacron blue are extending outside the surface of the enzyme (Figure 5; compare panel E with panels C and D).

DISCUSSION

We report here the crystal structure of the human NQO1 in complex with dicouamrol at 2.75 Å resolution. Analysis

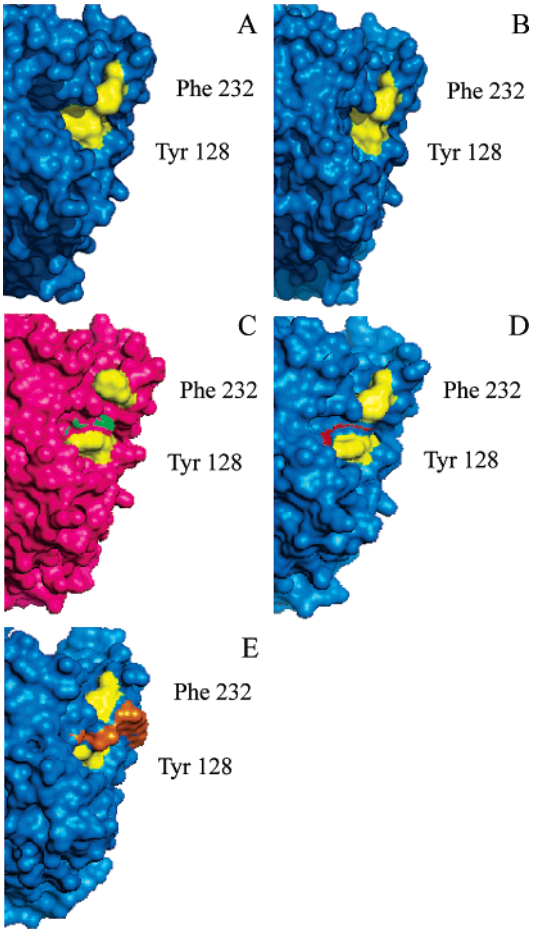

FIGURE 5: Comparison of the surface of NQO1 upon binding of different inhibitors and a substrate. (A) Apo hNQO1 colored in blue (PDB accession code 1D4A). (B) hNQO1 colored in blue with duroquinone colored in green, not apparent on the surface (PDB accession code 1DXO). (C) hNQO1 colored in pink with dicoumarol colored in green. (D) hNQO1 colored in blue with ES936 colored in red (PDB accession code 1KBQ). (E) Rat NQO1 colored in blue with Cibacron blue colored in orange (PDB accession code 1QRD). Tyr 128 and Phe 232 are labeled and colored in yellow.

of the hNQO1−dicoumarol crystal structure shows that one coumarin ring of dicoumarol stacks parallel to the isoalloxazine ring of FAD and forms hydrogen bonds with Tyr 128 and His 161. Comparison of the hNQO1−dicoumarol structure with the apo hNQO1 structure shows that, upon binding of dicoumarol, there is a significant movement of two residues in the catalytic pocket, Tyr 128 and Phe 232. This movement is probably critical for the entrance and binding of dicoumarol to the enzyme active site.

Our hNQO1−dicoumarol structure is in line with previous mutational studies of human and rat NQO1, which shares 86% amino acid sequence homology with human NQO1. Previous mutational analysis of the rat NQO1 showed that replacement of tyrosine 128 with valine increases the K_i value for dicoumarol about 12-fold (*22*). Replacement of tyrosine 128 with aspartic acid further increases the K_i value for dicoumarol about 70-fold (*9*). Our hNQO1−dicoumarol structure provides a structural basis for the observation that Tyr 128 is important for dicoumarol binding and demonstrates that Tyr 128 is positioned in close vicinity to dicoumarol (3.26 Å) and forms a hydrogen bond with dicoumarol. We also identified another hydrogen bonds between dicouamrol and His 161. Indeed, mutation of His 161 to Gln in the human NQO1 increases the K_i value for dicoumarol from 0.5 to 70 nM (*9*). Gly 150 is another residue that plays an important role in the binding of dicoumarol to NQO1. Replacement of Gly 150 with valine in the rat NQO1 strongly increases the K_i value for dicoumarol from 2 to 970 nM (*9*). Our hNQO1−dicouamrol structure clearly shows that Gly 150 is in close vicinity to dicoumarol (3.3 Å) and might form a hydrophobic interaction with dicoumarol.

The crystal structure of hNQO1 in complex with dicoumarol also provides insight into the mechanism of NQO1 interaction with the tumor suppressors p53 and p73α and with ODC, since the binding of NQO1 to these proteins is disrupted in the presence of dicoumarol (*16*, *18*, *21*). Our results indicate that the structural changes that occur upon binding of dicoumarol to NQO1 are limited to the active site of NQO1 (Figure 4, panel A). Therefore, the ability of dicoumarol to disrupt the binding of NQO1 to p53, p73α, and ODC suggests that the binding is dependent on the active site conformation. The major changes that occur within the active site are in positions of Tyr 128 and Phe 232. The distance between these two residues significantly increases from about 5 Å in the apo hNQO1 to 12 Å in the hNQO1 bound to dicoumarol. Previously, we showed that Tyr 128 of NQO1 is essential for p53 and p73α binding because its replacement by valine or phenylalanine abrogates the binding to p53 and p73α (*18*). Therefore, we propose that the observed dicoumarol-induced conformational changes in the positions of Tyr 128 and Phe 232 on the surface of NQO1 might interfere with the binding of NQO1 to p53, p73α, and ODC.

ES936 is a mechanism-based inhibitor that inhibits NQO1 activity by alkylating either tyrosine 126 or tyrosine 128 in the active site of NQO1 (*11*). In contrast to dicoumarol, Cibacron blue, and several other competitive inhibitors of NQO1 activity, ES936 was reported neither to induce p53 degradation nor to inhibit p53−NQO1 binding (*16*, *21*). It is interesting that the hNQO1−ES936 structure exhibits a more limited movement of both Tyr128 and Phe 232 compared to the hNQO1−dicoumarol structure. Such a limited movement might be insufficient to disrupt the binding of NQO1 to p53. While a similar degree of limited movement was observed in the case of Cibacron blue, that induces p53 degradation although less effectively than dicoumarol (*16*). However, Cibacron blue is a larger molecule that extensively protrudes from the surface of NQO1. This generates additional steric effects that might interfere with the binding of NQO1 to p53, even if the position of Tyr 128 and Phe 232 still enables such association. Although less effective than dicoumarol, several additional NQO1 inhibitors, including chrysin, DHF, and curcumin, block the ability of NQO1 to stabilize its interacting proteins (*16*, *21*). The resolution of the NQO1 structure in complex with these different inhibitors should provide useful information to substantiate the proposed model.

We have previously shown that the binding of NQO1 to p53 and p73α is increased in the presence of NADH. Dicoumarol disrupts the binding of NQO1 to p53 and p73α and induces ubiquitin-independent proteasomal degradation of these proteins (*18*). Several other competitive inhibitors of NQO1, which compete with NADH, induce p53 degrada-

tion and inhibit p53-dependent apoptosis (*16*). Thus, NADH not only serves as an electron donor in the enzymatic activity of NQO1 but also promotes the binding of NQO1 to p53 and p73α possibly by inducing a conformation that favors these interactions. It is also possible that NQO1-associated NADH plays a direct role in binding of the client proteins.

The binding of NQO1 to p73α is mediated via its C-terminal SAM domain. p73*β*, a p73 isoform that lacks the C-terminal SAM domain, does not bind to NQO1 whereas the C-terminal SAM domain itself is sufficient for NQO1 binding (*18*). p53 shares significant homology with p73, in particular with p73*β*, and does not harbor a SAM domain; however, it binds NQO1 with affinity similar to that of p73α (*18*). Furthermore, the "hot spot" p53 mutants, p53 R175H and p53 R273H, exhibit increased binding of NQO1 compared to wild-type p53, and the ability of dicoumarol to disrupt their binding to NQO1 is reduced (*12*, *16*). Finally, NQO1 also binds the enzyme ODC which does not share any significant structural homology with p53 or p73α (*19*). However, the fact that dicoumarol disrupts the binding of these different proteins to NQO1 suggests that they all share a common binding site on NQO1 (*18*, *19*). Thus, it seems that a defined region within NQO1 is capable of binding different protein substrates with different structural requirements.

The crystal structure of hNQO1−dicoumarol described here and the comparison to the NQO1 structure in the presence of other NQO1 inhibitors provide a useful tool for understanding the mechanism of action of the different inhibitors and for the development and identification of additional potent inhibitors of NQO1 activity. Furthermore, analysis of the hNQO1−dicoumarol structure provides the first step in the molecular understanding of NQO1 interaction with p53 and other short-lived proteins.

ACKNOWLEDGMENT

We thank the Israel Structural Proteomics Center (ISPC) members Dr. T. Unger, Dr. S. Albeck, and Dr. Y. Peleg for the purification and crystallization of NQO1. We also thank Dr. J. Sussman, Dr. D. Tawfik, Dr. I. Pecht, and Dr. J. Lotem for critical review and advice.

REFERENCES

1. Lind, C., Cadenas, E., Hochstein, P., and Ernster, L. (1990) DT-diaphorase: purification, properties, and function, *Methods Enzymol. 186*, 287−301.
2. Joseph, P., Long, D. J., Jr., Klein-Szanto, A. J., and Jaiswal, A. K. (2000) Role of NAD(P)H:quinone oxidoreductase 1 (DT diaphorase) in protection against quinone toxicity, *Biochem. Pharmacol. 60*, 207−214.
3. Siegel, D., Gibson, N. W., Preusch, P. C., and Ross, D. (1990) Metabolism of mitomycin C by DT-diaphorase: role in mitomycin C-induced DNA damage and cytotoxicity in human colon carcinoma cells, *Cancer Res. 50*, 7483−7489.
4. Pink, J. J., Planchon, S. M., Tagliarino, C., Varnes, M. E., Siegel, D., and Boothman, D. A. (2000) NAD(P)H:quinone oxidoreductase activity is the principal determinant of beta-lapachone cytotoxicity, *J. Biol. Chem. 275*, 5416−5424.
5. Li, R., Bianchet, M. A., Talalay, P., and Amzel, L. M. (1995) The three-dimensional structure of NAD(P)H:quinone reductase, a flavoprotein involved in cancer chemoprotection and chemotherapy: mechanism of the two-electron reduction, *Proc. Natl. Acad. Sci. U.S.A. 92*, 8846−8850.
6. Hosoda, S., Nakamura, W., and Hayashi, K. (1974) Properties and reaction mechanism of DT diaphorase from rat liver, *J. Biol. Chem. 249*, 6416−6423.
7. Garten, S., and Wosilait, W. D. (1971) Comparative study of the binding of coumarin anticoagulants and serum albumins, *Biochem. Pharmacol. 20*, 1661−1668.
8. Chen, S., Hwang, J., and Deng, P. S. (1993) Inhibition of NAD(P)H:quinone acceptor oxidoreductase by flavones: a structure−activity study, *Arch. Biochem. Biophys. 302*, 72−77.
9. Chen, S., Wu, K., Zhang, D., Sherman, M., Knox, R., and Yang, C. S. (1999) Molecular characterization of binding of substrates and inhibitors to DT-diaphorase: combined approach involving site-directed mutagenesis, inhibitor-binding analysis, and computer modeling, *Mol. Pharmacol. 56*, 272−278.
10. Prestera, T., Prochaska, H. J., and Talalay, P. (1992) Inhibition of NAD(P)H:(quinone-acceptor) oxidoreductase by cibacron blue and related anthraquinone dyes: a structure−activity study, *Biochemistry 31*, 824−833.
11. Winski, S. L., Faig, M., Bianchet, M. A., Siegel, D., Swann, E., Fung, K., Duncan, M. W., Moody, C. J., Amzel, L. M., and Ross, D. (2001) Characterization of a mechanism-based inhibitor of NAD(P)H:quinone oxidoreductase 1 by biochemical, X-ray crystallographic, and mass spectrometric approaches, *Biochemistry 40*, 15135−15142.
12. Tsvetkov, P., Asher, G., Reiss, V., Shaul, Y., Sachs, L., and Lotem, J. (2005) Inhibition of NAD(P)H:quinone oxidoreductase 1 activity and induction of p53 degradation by the natural phenolic compound curcumin, *Proc. Natl. Acad. Sci. U.S.A. 102*, 5535−5540.
13. Asher, G., Lotem, J., Cohen, B., Sachs, L., and Shaul, Y. (2001) Regulation of p53 stability and p53-dependent apoptosis by NADH quinone oxidoreductase 1, *Proc. Natl. Acad. Sci. U.S.A. 98*, 1188−1193.
14. Asher, G., Lotem, J., Kama, R., Sachs, L., and Shaul, Y. (2002) NQO1 stabilizes p53 through a distinct pathway, *Proc. Natl. Acad. Sci. U.S.A. 99*, 3099−3104.
15. Asher, G., Lotem, J., Sachs, L., Kahana, C., and Shaul, Y. (2002) Mdm-2 and ubiquitin-independent p53 proteasomal degradation regulated by NQO1, *Proc. Natl. Acad. Sci. U.S.A. 99*, 13125−13130.
16. Asher, G., Lotem, J., Tsvetkov, P., Reiss, V., Sachs, L., and Shaul, Y. (2003) P53 hot-spot mutants are resistant to ubiquitin-independent degradation by increased binding to NAD(P)H:quinone oxidoreductase 1, *Proc. Natl. Acad. Sci. U.S.A. 100*, 15065−70.
17. Asher, G., Lotem, J., Sachs, L., and Shaul, Y. (2004) p53-dependent apoptosis and NAD(P)H:quinone oxidoreductase 1, *Methods Enzymol. 382*, 278−293.
18. Asher, G., Tsvetkov, P., Kahana, C., and Shaul, Y. (2005) A mechanism of ubiquitin-independent proteasomal degradation of the tumor suppressors p53 and p73, *Genes Dev. 19*, 316−321.
19. Asher, G., Bercovich, Z., Tsvetkov, P., Shaul, Y., and Kahana, C. (2005) 20S proteasomal degradation of ornithine decarboxylase is regulated by NQO1, *Mol. Cell 17*, 645−655.
20. Asher, G., and Shaul, Y. (2005) p53 proteasomal degradation: poly-ubiquitination is not the whole story, *Cell Cycle 4*, 1015−1018.
21. Anwar, A., Dehn, D., Siegel, D., Kepa, J. K., Tang, L. J., Pietenpol, J. A., and Ross, D. (2003) Interaction of human NAD(P)H:quinone oxidoreductase 1 (NQO1) with the tumor suppressor protein p53 in cells and cell-free systems, *J. Biol. Chem. 278*, 10368−10373.
22. Ma, Q., Cui, K., Xiao, F., Lu, A. Y., and Yang, C. S. (1992) Identification of a glycine-rich sequence as an NAD(P)H-binding site and tyrosine 128 as a dicumarol-binding site in rat liver NAD(P)H:quinone oxidoreductase by site-directed mutagenesis, *J. Biol. Chem. 267*, 22298−22304.
23. Otwinowski, Z., and Minor, W. (1997) Processing of X-ray diffraction data collected in oscillation mode, *Methods Enzymol. 276*, 307−326.
24. Storoni, L. C., McCoy, A. J., and Read, R. J. (2004) Likelihood-enhanced fast rotation functions, *Acta Crystallogr., Sect. D: Biol. Crystallogr. 60*, 432−438.
25. Brunger, A. T., Adams, P. D., Clore, G. M., DeLano, W. L., Gros, P., Grosse-Kunstleve, R. W., Jiang, J. S., Kuszewski, J., Nilges, M., Pannu, N. S., Read, R. J., Rice, L. M., Simonson, T., and Warren, G. L. (1998) Crystallography & NMR system: A new software suite for macromolecular structure determination, *Acta Crystallogr., Sect. D: Biol. Crystallogr. 54* (Part 5), 905−921.

26. Jones, T. A., Zou, J. Y., Cowan, S. W., and Kjeldgaard. (1991) Improved methods for building protein models in electron density maps and the location of errors in these models, *Acta Crystallogr. A47* (Part 2), 110−119.
27. Laskowski, R. A., MacArthur, M. W., Moss, D. S., and Thornton, J. M. (1993) PROCHECK: a program to check the stereochemical quality of protein structures, *J. Appl. Crystallogr. 26*, 283−291.
28. Faig, M., Bianchet, M. A., Talalay, P., Chen, S., Winski, S., Ross, D., and Amzel, L. M. (2000) Structures of recombinant human and mouse NAD(P)H:quinone oxidoreductases: species comparison and structural changes with substrate binding and release, *Proc. Natl. Acad. Sci. U.S.A. 97*, 3177−3182.
29. Wallace, A. C., Laskowski, R. A., and Thornton, J. M. (1995) LigPlot: a program to generate schematic diagrams of protein−ligand interactions, *Protein Eng. 8*, 127−134.

BI0600087